ELSEVIER

Journal of University of Science and Technology Beijing
Volume 15, Number 4, August 2008, Page 461

Materials

Preparation of IrO_2+MnO_2 coating anodes and their application in NaClO production

Yongle Ni, Huimin Meng, Dong Chen, Dongbai Sun, and Hongying Yu

School of Materials Science and Engineering, University of Science and Technology Beijing, Beijing 100083, China

(Received 2007-09-16)

Abstract: To improve the durability as well as to reduce the cost of anodes, the IrO_2+MnO_2 composite coating anodes for NaClO production were prepared by thermal decomposition. Scanning electron microscopy (SEM), energy dispersive X-ray spectroscopy (EDX), and X-ray diffraction analysis (XRD) were carried out to investigate the morphologies, element distribution, and microstructure. The anodic polarization curves were employed to study the effect of sintering temperature on the Cl_2 evolution reaction (CER) of the electrodes. The accelerated life tests (ALT) and electrochemical impedance spectroscopy measurement (EIS) were utilized to investigate the stability. The rules of NaClO production were also studied by the static electrolysis experiment. The results indicate that sintering temperature has a significant influence on the CER properties as well as the ALT values of the electrodes. The electrode prepared at 400°C has the best CER properties and the longest ALT value.

Key words: iridium dioxide; manganese dioxide; sodium hypochlorite; chlorine evolution; stability; impedance spectroscopy measurement (EIS)

1. Introduction

NaClO has been widely used as a highly effective and low-cost biocide. NaClO can be produced by infusing chlorine gas into a cold solution of NaOH or by electrolyzing NaCl solution. Concentrated sodium hypochlorite is hyper-unstable, and the available chlorine in the solution rapidly decreases during storage and transportation [1]. Therefore, the on-site production of sodium hypochlorite by electrolyzing NaCl solution is an effective way to avoid this shortcoming.

The electrodes widely used in the hypochlorite production by electrolyzing are RuO_2·TiO_2/Ti and Pt/Ti [2-3]. Though traditional RuO_2·TiO_2/Ti anode performs the best electrocatalytic activity among all kinds of dimensional stable anodes (DSA), it suffers oxidation and corrosion owing to the unavoidable oxygen evolution [4] for NaClO production. Therefore, the accelerated life test (ALT) value of RuO_2·TiO_2/Ti in NaClO production is limited. Pt/Ti shows a higher overpotential in NaClO production and the cost is very high.

Both IrO_2 and MnO_2 have rutile structures and have been widely used in industries. MnO_2 with excellent anti-corrosion properties in several media and low-price has attracted attention for use as an insoluble anode both for chlorine evolution and oxygen evolution and is regarded as a DSA material with bright future [5]. MnO_2 was obtained by thermal decomposition or by anodic electric deposition [6-8]. The IrO_2 anode was also widely used as the anodic material both for oxygen evolution and chlorine evolution [9-10].

In this article, the IrO_2+MnO_2 mixed anodes mostly comprised of low cost MnO_2 which was used to substitute noble metals or metallic oxide anodes. To avoid the formation of insulating titanium oxide between the substrate and the active oxide coating, the titanium substrate was coated with the SbO_x+SnO_2 coatings as intermediate layers. The effect of sintering temperature on the catalytic activity and durability was investigated by means of electrochemical impedance spectroscopy measurement (EIS), cyclic voltammetry (CV), and ALT.

2. Experimental

2.1. Electrode preparation

A conventional thermal-decomposition was em-

Corresponding author: Yongle Ni, **E-mail:** nyl_ustb@126.com
Also available online at www.sciencedirect.com

ployed to prepare the IrO_2+MnO_2 coating. To achieve a favorable roughness and maintain the cleanness of titanium plates (TA1) that were used as the substrate, prior to the process, the titanium plates were sand-blasted and degreased, and then etched in 10wt% oxalic acid, finally rinsed with distilled water in an ultrasonic bath and dried in a hot air stream. The SnO_2+SbO_x intermediates (three layer) were prepared through the decomposition of the $SnCl_4$ and $SbCl_3$ precursors in alcoholic solution. After painting the SbO_x+SnO_2 intermediates, the substrates were brushed with the 0.2 mol·dm^{-3} aqueous solution containing H_2IrCl_6 and Mn $(NO_3)_2$ (Ir:Mn=10:90, mol%). After being dried at 100°C, the substrates were heated at certain annealing temperature for 10 min. The whole procedure was repeated 20 times. A final calcination at certain annealing temperature for 30 min completed the treatment.

2.2. Material characterization

The surface morphologies of the prepared anodes were investigated using a Cambridge S360 scanning electron microscope (SEM), and the element distribution was determined using an EVEX Sigma energy dispersive X-ray spectroscope (EDX). The microstructural investigation was carried out by X-ray diffraction analysis (XRD) of the prepared anodes. These analyses were performed on a Siemens D5000 instrument using Cu K_α radiation and nickel filter.

2.3. Accelerated life tests

The accelerated electrolysis was carried out in the 0.5 mol·dm^{-3} H_2SO_4 solution under galvanostatic electrolysis at a current density of 200 A·dm^{-3} at room temperature. Ti plates were used as the counter electrodes. The service life was cumulated until the cell voltage increased to 5 V.

2.4. Electrochemical measurement

A single three-electrode compartment cell system was employed. The anode surface was in a vertical plane to avoid the accumulation of gas bubbles. A platinum plate was used as the counter electrode, with KCl saturated calomel electrode (SCE) as the reference. All the electrochemical measurements were maintained at 25°C with a CHI660B electrochemical workstation. The cyclic voltammetry curves were recorded between the potential domain of hydrogen evolution and chlorine evolution in 1 mol·dm^{-3} NaCl at the sweep rate of 10 mV·s^{-1}. The anodic polarization curves were recorded in 1 mol·dm^{-3} NaCl at the sweep rate of 10 mV·s^{-1}. The electrochemical impedance measurement was carried out in the 0.5 mol·dm^{-3} H_2SO_4 solution for the electrode after accelerated electrolysis for different time in the frequency range of 10^{-2} to 10^5 Hz. The amplitude of the AC signal was 5 mV and the operating potential was selected as 1.2 V. The impedance data were converted into the Nyquist data format, and then fitted to appropriate simulative circuits.

2.5. NaClO production

A single compartment cell with two electrodes vertically immersed into the solution was employed as the electrochemical reactor. Ti plates were used as the cathodes. The 200-mL dilute NaCl solution with certain concentration was used as the electrolyte. According to GB12176-90, available chlorine concentration (ACH) was determined by iodometric titration .The electric current efficiency η is defined as the ratio of the experimental chlorine production to the theoretical chlorine production. The production rate of available chlorine can be calculated as follows:

$$v = 2.65\eta \quad (\mathrm{g \cdot A^{-1} \cdot h^{-1}}) \tag{1}$$

3. Results and discussion

3.1. Material characterization by XRD, SEM, and EDX

X-ray diffraction patterns of the prepared IrO_2+MnO_2 coatings at various sintering temperatures are shown in Fig. 1. At low temperatures (equal or lower than 350°C), several unidentifiable and weak reflections are observed, reflecting that the thermal decomposition produced a mixed oxide of low crystalline degree. This behavior can imply the fact that the annealing temperature necessary to transform all precursors into dioxide is higher than 350°C in the experimental conditions employed. At high temperatures (equal or higher than 500°C), single rutile-type IrO_2 and MnO_2 intensive diffraction peaks are shaped. Only three main broad and weak peaks are formed at sintering temperatures of 400 and 450°C. Since both rutile-type IrO_2 and MnO_2 are of tetragonal structure and share similar crystal lattice constant, it can be concluded that the mixed oxide forms a solid solution of IrO_2 and MnO_2 with the rutile-type structure at 400 and 450°C. Hu [11] indicated that the high stability of 30wt% IrO_2+70wt% Ta_2O_5 was mainly contributed to the highest proportion of solid solution of the IrO_2+Ta_2O_5 mixed oxide, and therefore, the formed rutile-type solid solution of IrO_2 and MnO_2 could benefit the stability of the IrO_2+MnO_2 electrodes.

SEM micrographs of the prepared IrO_2+MnO_2 anodes at various sintering temperatures are shown in Fig. 2. Though the surfaces of all specimens are composed of cracks, pits, and agglomerations (bright par-

ticles), their surface morphologies are quite different from each other. Coarse grains and a small amount of agglomerations were investigated on the surface of the specimen prepared at the sintering temperature of 350°C, representing the state of incomplete decomposition with the characterization of poor crystallization. At sintering temperatures of 400°C and 450°C, the grain size of the specimen is considerably smaller than that of the sample prepared at lower temperature and the amount of agglomerations is significantly increased. While the surface of the sample prepared at 500°C is quite different from others. There are few agglomerations on the surface. It is seen that the presence of agglomerations is inhibited at high temperature [12]. The results indicate that more electrochemical surface areas are obtained at 400°C and 450°C, implying a better electrocatalytic activity.

EDX was utilized to analyze the whole surface and the typical areas of the oxide surface. The results are listed in Table 1. The EDX analysis shows that the iridium enrichment oxide coatings in the surface are obtained at sintering temperatures of 400 and 450°C, which is mainly owing to the formation of the IrO_2+MnO_2 solid solution. It also reveals that the bright areas are enriched with iridium. Since the electrocatalytic activity of IrO_2 is considerably better than that of MnO_2, the higher electrocatalytic activity of the samples prepared at 400 and 450°C can also be forecasted.

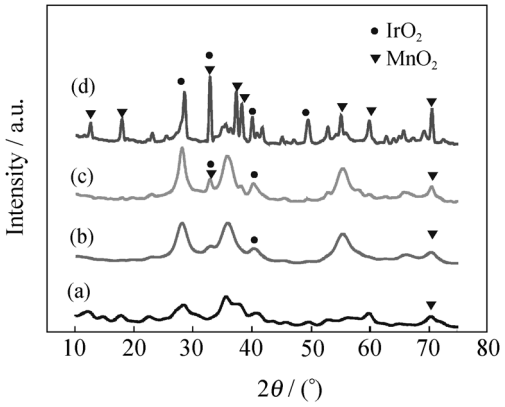

Fig. 1. XRD patterns of the IrO_2+MnO_2 electrodes at various sintering temperatures: (a) 350°C; (b) 400°C; (c) 450°C; (d) 500°C.

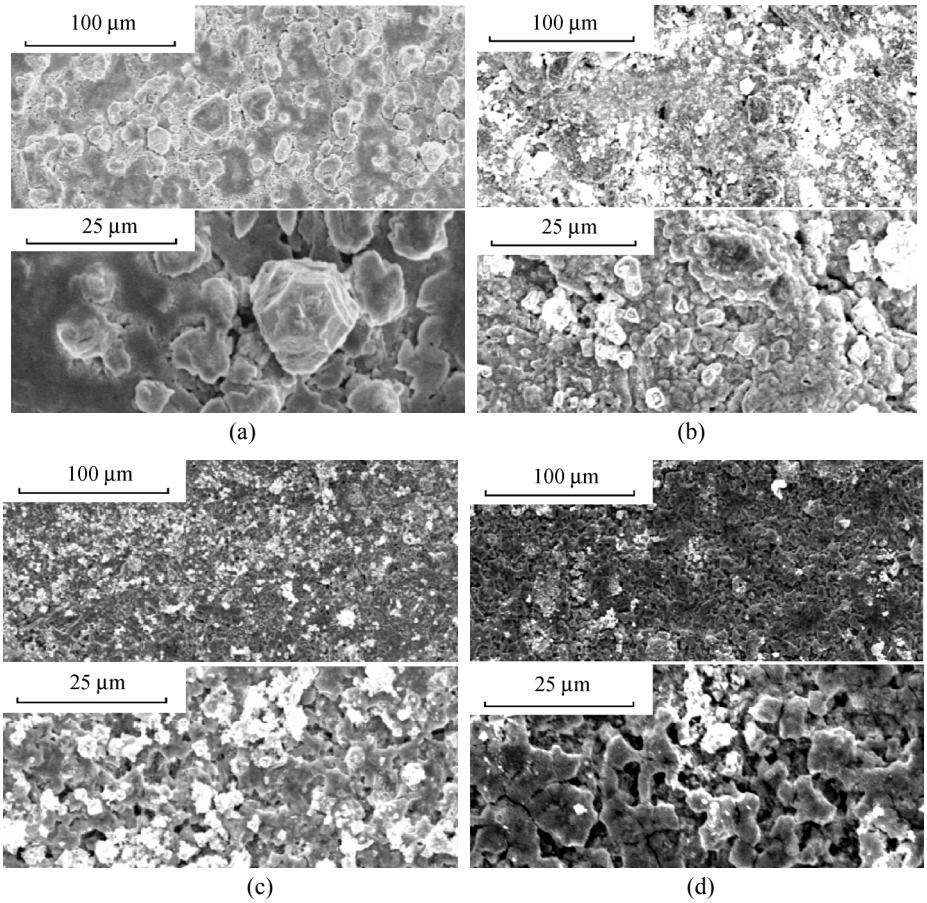

Fig. 2. SEM micrographs of the IrO_2+MnO_2 electrodes at various sintering temperatures: (a) 350°C; (b) 400°C; (C) 450°C; (d) 500°C.

3.2. Electrocatalytic activities

The chlorine evolution reaction on the IrO_2+MnO_2 electrodes prepared at various sintering temperatures was investigated by anodic polarization curves, which were measured in 1 mol·dm^{-3} NaCl at the sweep rate

of 10 $mV \cdot s^{-1}$, and the curves are shown in Fig. 3. The result depicts that the chlorine evolution reaction commences at 1.1 V *vs.* SCE with the IrO_2+MnO_2 electrodes prepared at various temperatures. The IrO_2+MnO_2 electrodes prepared at 400 and 450°C are considerably more active than the electrodes prepared at 350 and 500°C. The IrO_2+MnO_2 electrode prepared at 400°C shows the best electrocatalytic activity. The result is mainly owing to the more content of iridium on the surface of the IrO_2+MnO_2 electrode prepared at 400°C. The IrO_2+MnO_2 electrodes prepared at 350 and 500°C show considerably lower electrocatalytic activities resulting from the incomplete decomposition.

Table 1. Atom percentage obtained from EDX for the IrO_2+MnO_2 electrodes prepared at various sintering temperatures at%

Temperature / °C	Global areas		Bright areas	
	Ir	Mn	Ir	Mn
350	7.6663	92.3337	14.5595	85.4405
400	15.7634	84.2366	38.8218	61.1782
450	14.1184	85.8816	26.6271	73.3729
500	6.4194	93.5803	15.7094	84.2906

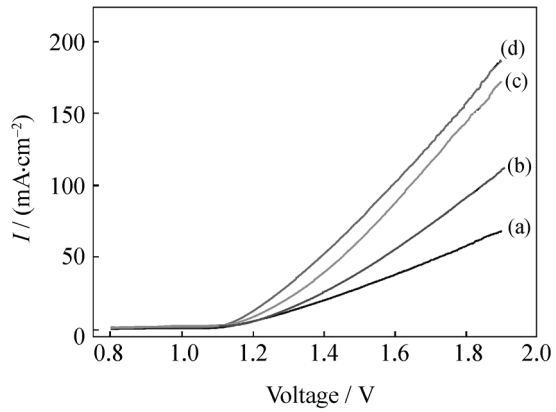

Fig. 3. Polarization curves measured in 1 $mol \cdot dm^{-3}$ NaCl at the sweep rate of 10 $mV \cdot s^{-1}$ of the IrO_2+MnO_2 electrodes prepared at various sintering temperatures: (a) 350°C; (b) 400°C; (c) 450°C; (d) 500°C.

3.3. Investigation of stability properties

(1) *E versus t* curves.

The ALT showed that the sample prepared at 400°C also exhibits the most excellent stability. The cell voltage *E versus* electrolysis time curves for the IrO_2+MnO_2 electrode prepared at 400°C, representing the anode deactivate course, are shown in Fig. 4. During the initial stage of electrolysis, the cell voltage decreases, which is mainly owing to the gradual wetting of the inner porosity of the composite electrode during the electrolysis. Then, the cell voltage remains constant from 20 to 340 h, which is the major part of the electrolysis time. Finally, the cell voltage increases rapidly until the electrode loses its activity, suggesting the complete deactivation of the electrode. This result indicates that the electrode is stable and the coating wear is slow and uniform during the electrolysis.

(2) *In situ* cyclic voltammetric (CV) analysis.

The changes suffered by the electrode surface during the ALT experiment can be tracked by the *in situ* CV curves at different electrolysis times [13]. The CV behavior of the IrO_2+MnO_2 electrode prepared at 400°C *versus* electrolysis time is shown in Fig. 5. A decrease in voltammetric current with increasing electrolysis time is observed; however, the voltammetric profile does not change, suggesting that the electrochemically active surface area of the electrode does not change significantly and reflecting a uniform and slow electrode wear during electrolysis. This result also shows that after electrode deactivation, a significant amount of catalyst is still present in the coating.

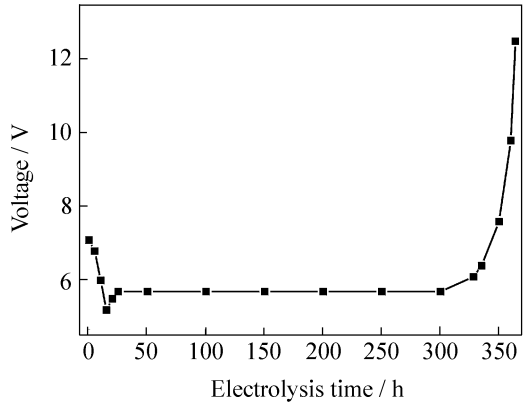

Fig. 4. Cell voltage *versus* electrolysis time at the current of 2 $A \cdot cm^{-2}$ in 0.5 $mol \cdot dm^{-3}$ H_2SO_4.

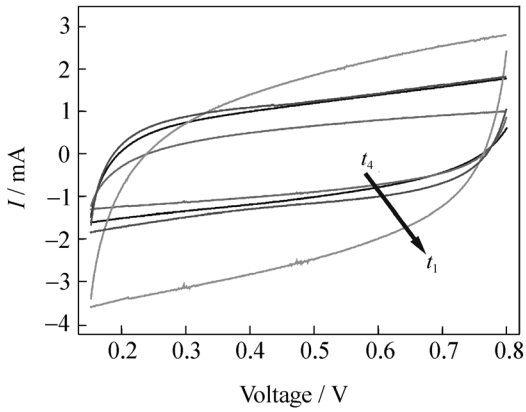

Fig. 5. CV behavior *versus* electrolysis time: t_1=20 h; t_2=100 h; t_3=300 h; t_4=364 h (deactivation) (electrolyte: 1 $mol \cdot dm^{-3}$ NaCl; V=10 $mV \cdot s^{-1}$).

(3) EIS analysis.

Fig. 6 shows the effect of the complex plane of the electrochemical impedance behavior as well as the simulated data on the electrolysis time of the anodes. The experimental data are accurately fitted to an R_S

(R_fQ_f) ($R_{ct}Q_{dl}$) equivalent circuit [13-14]. In this circuit, (R_fQ_f) describes the properties of the oxide film, whereas ($R_{ct}Q_{dl}$) is related to the behavior of the interface between oxide and electrolyte. Here, R_f is the resistance of the interfacial TiO_2 film localized in the Ti/oxide interlayer, R_{ct} the charge transfer resistance for oxygen evolution. Constant phase elements Q_f and Q_{dl} are employed to replace the film capacitance and double layer capacitance, respectively, owing to the porous structure of the oxide electrode. R_S refers to the uncompensated solution resistance. The parameters obtained by simulation are listed in Table 2.

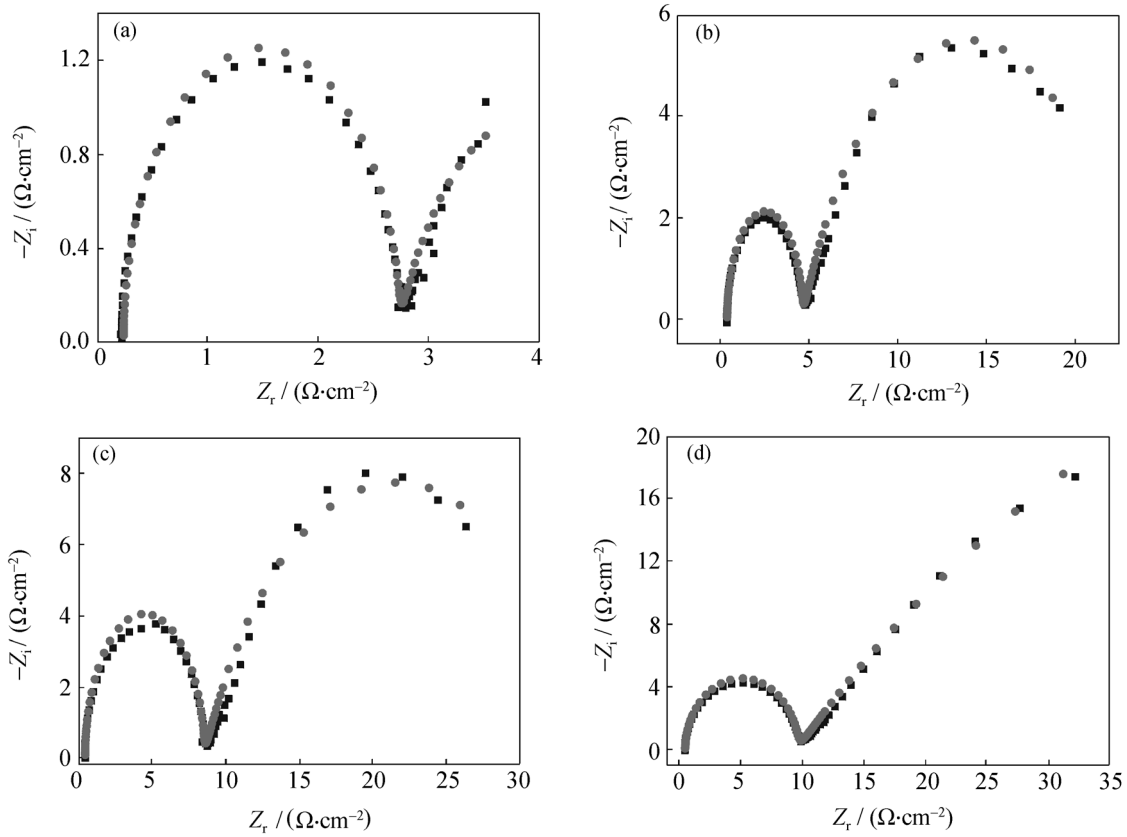

Fig. 6. Complex planes of the Ti/SbO_x+SnO_2/IrO_2+MnO_2 electrode after different times of electrolysis: (a) 20 h; (b) 100 h; (c) 300 h; (d) 364 h (electrolyte: 0.5 mol·dm^{-3} H_2SO_4; ♦ experimental data; ● simulation data; *E*=1.20 V *vs.* SCE).

Table 2. Impedance parameters for the accelerated electrolysis test of the Ti/SbO_x+SnO_2/IrO_2+MnO_2 anodes obtained by fitting the experiment data to the equivalent circuit

Electrolysis time / h	R_s / (Ω·cm^{-2})	R_f / (Ω·cm^{-2})	Q_f / (mF·cm^{-2})	n_1	R_{ct} / (Ω·cm^{-2})	Q_{dl} / (mF·cm^{-2})	n_2
20	0.161	2.54	6.13×10^{-2}	1.0	7.42	67.6	0.72
100	0.363	4.19	3.24×10^{-2}	1.0	18.57	37.8	0.68
300	0.219	7.82	1.52×10^{-2}	1.0	35.69	18.8	0.74
364	0.187	10.2	1.25×10^{-2}	1.0	245.2	10.9	0.80

From Table 2, it can be seen that R_f continues to rise during the whole course of electrolysis, implying a large film resistance between the MnO_2 oxide and Ti substrate resulting from the passivation of Ti base during the electrolysis, while Q_{dl} changes in a different trend. Q_{dl} can be viewed as the pseudo-capacitance of the double layer, since the power factor n_2 related to the depression angle of Q_{dl} is in the range of 0.6~0.8 at different times of electrolysis. The change trend of Q_{dl} also reflects the decrease of active surface area during the course of electrolysis [15].

When the cell voltage increased 5 V at the end of the electrolysis test, R_f reached 10.2 Ω·cm^{-2}, a typical value representing the passivation of the titanium substrate [15-18]. A significant amount of catalyst (shown in the CV curves) that remained after the accelerated life test also confirms that the major reason of the electrode deactivation is the passivation of the Ti substrate, while the active oxide coating suffers corrosion and erosion during the whole electrolysis.

3.4. NaClO production

The IrO_2+MnO_2 electrode with the best electrocatalytic activity prepared at 400°C was used as the

anode for NaClO production. The factors that influenced the concentration of available chlorine and electric current efficiency such as salt concentration, temperature, and current density were studied through a static experiment without a membrane.

The effect of salt concentration on the ACH is shown in Fig. 7. The ACH increases with the increase in the NaCl content, while the content of NaCl is higher than 60 $g \cdot L^{-1}$, the ACH is leveled off. From a pragmatic point, the NaCl content of 60 $g \cdot L^{-1}$ will be a better choice.

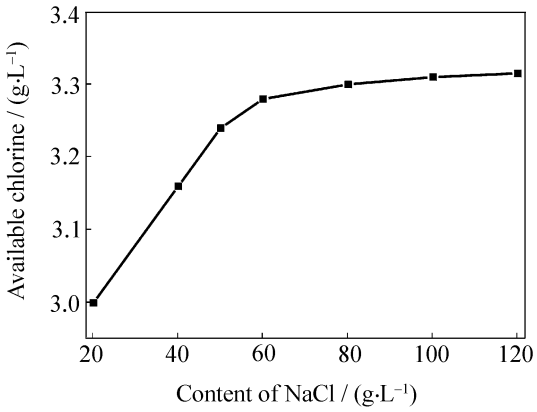

Fig. 7. Effect of NaCl content on the concentration of available chlorine (current density: 10 $A \cdot dm^{-2}$; temperature: 20°C; electrolysis time: 1 h).

Fig. 8 shows the influence of temperature on the ACH. It reveals that the ACH decreases dramatically with the increase in temperature. Thus, the electrolysis process should be carried out at a lower temperature to retard the sub-reaction and decomposition of NaClO as well as to ease the Cl_2 dissolving.

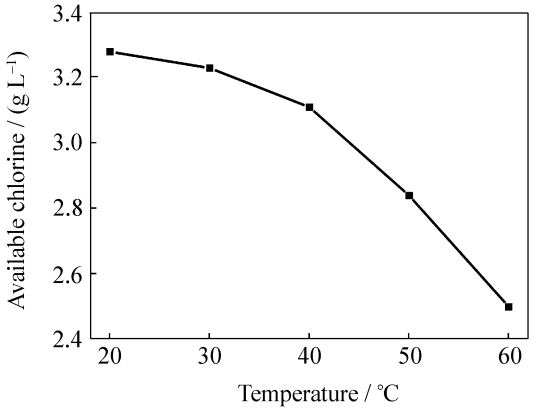

Fig. 8. Effect of temperature on the concentration of available chlorine (NaCl content: 60 $g \cdot L^{-1}$; electrolysis time: 1 h).

Fig. 9 represents the effect of current density on the concentration of available chlorine. The available chlorine concentration rises almost linearly with the increase in current density, while at higher current densities such as 20 and 25 $A \cdot dm^{-2}$, the increase rate is slightly slow. This phenomenon is coursed by the oxygen evolution, which is evolved at higher current densities. To keep a high current efficiency, a comparatively lower current density should be employed.

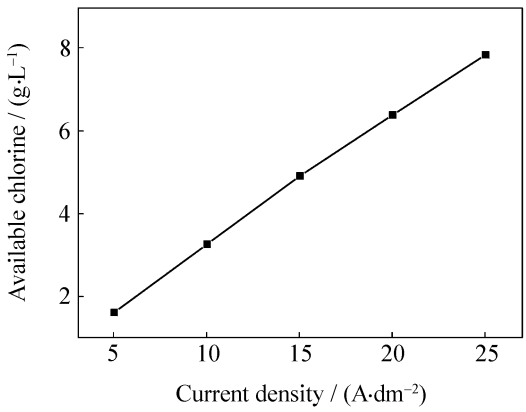

Fig. 9. Effect of current density on the concentration of available chlorine (temperature: 20°C; NaCl content: 60 $g \cdot L^{-1}$; electrolysis time: 1 h).

The electric current efficiency reaches a maximum and equals 72.4% when electrolyzing the solution with a NaCl content of 60 $g \cdot L^{-1}$ at 20°C, and the production rate of available chlorine is 1.92 $g \cdot A^{-1} \cdot h^{-1}$. The prepared IrO_2+MnO_2 electrode with low cost shows a good activity of chlorine evolution and is a good substitute for NaClO production. When the prepared electrode is used as the anode for NaClO production in proper conditions, its electric current efficiency is as high as RuO_2 [3], which is claimed as the best material for chlorine evolution and is widely used in the chlorine-alkali industry.

4. Conclusions

(1) Low-cost IrO_2+MnO_2 composite coating electrodes were prepared by thermal-decomposition; SEM, EDX, and XRD analysis shows that a higher active surface as well as more iridium content on the surface is obtained when the electrodes were prepared at sintering temperatures of 400 and 450°C.

(2) The IrO_2+MnO_2 composite coating electrode prepared at 400°C represents the best electrocatalytic activity in the chlorine evolution reaction owing to the comparatively large active surface and the highest iridium content on the surface.

(3) The ALT carried out in 0.5 $mol \cdot dm^{-3}$ H_2SO_4 shows that the ALT value of the IrO_2+MnO_2 composite coating electrode prepared at 400°C has reached 364 h, representing excellent stability. EIS and CV analyses verify that the deactivation mechanism of the electrode is mainly owing to the passivation of the substrate, while the coating suffers slow corrosion during electrolysis.

(4) The electrode with the best electrocatalytic activity is used as an anode for NaClO production. The electric current efficiency reaches 72.4% and the production rate of available chlorine is 1.92 $g \cdot A^{-1} \cdot h^{-1}$ when electrolyzing the solution with a NaCl content of 60 $g \cdot L^{-1}$ at 20°C at the current density of 15 $A \cdot dm^{-2}$.

References

[1] F. Hua, J.R. West, and R.A. Barker, Modeling of chlorine decay in municipal water supplies, *Water Res.*, 33(1999), No.12, p.2735.

[2] A. Khelifa, S. Moulay, F. Hannane, S. Benslimene, and M. Hecini, Application of an experimental design method to study the performance of electrochlorination cells, *Desalination*, 160 (2004), No.1, p.91.

[3] G.F. Qin, Z.Y. Li, X.D. Chen, and A.B. Russell, An experimental study of a NaClO generator for anti-microbial applications in the food industry, *J. Food Eng.*, 54(2002), No.1, p.111.

[4] G.N. Martelli, R. Ornelas, and G. Faita, Deactivation mechanisms of oxygen evolving anodes at high current densities, *Electrochim. Acta*, 39(1994), No.11-12, p.1551.

[5] S. Ardizzone and S. Trasatti, Interfacial properties of oxides with technological impact in electrochemistry, *Adv. Colloid Interface Sci.*, 64(1996), p.173.

[6] M. Morita, C. Iwakura, and H. Tamura, The anodic characteristics of manganese dioxide electrodes prepared by thermal decomposition of manganese nitrate, *Electrochim. Acta*, 22(1977), No.2, p.325.

[7] J.P. Rethinaraj and S. Visvanathan, Anodes for the preparation of EMD and application of manganese dioxide coated anodes for electrochemicals, *Mater. Chem. Phys.*, 27(1991), No.4, p.337.

[8] H.T. Li, F. Zhang, and W.L. Li, An anode material used in the electrolysis of low-NaCl-content sea water to produce NaClO, *J. Guangdong Nonferrous Met.* (in Chinese), 11(2001), No.1, p.41.

[9] C.P. De Pauli and S. Trasatti, Composite materials for electrocatalysis of O_2 evolution: IrO_2+SnO_2 in acid solution, *J. Electroanal. Chem.*, 538-539(2002), No.1, p.145.

[10] A. de Oliveira-Sousa, M.A.S. da Silva, S.A.S. Machado, L.A. Avaca, and P. de Lima-Neto, Influence of the preparation method on the morphological and electrochemical properties of Ti/IrO_2-coated electrodes, *Electrochim. Acta*, 45(2000), No.27, p.4467.

[11] J.M. Hu, *A study on the Mechanisms of Oxygen Evolution and Degradation for Ti-based IrO_2+Ta_2O_5 Anodes* [Dissertation] (in Chinese), University of Science and Technology Beijing, Beijing, 2000, p.45.

[12] J.M. Hu, J.Q. Zhang, and C.N. Cao, Thermolytic formation and microstructure of IrO_2+Ta_2O_5 mixed oxide anodes from chlorine precursors, *Thermochim. Acta*, 403(2003), No.2, p.257.

[13] J.M. Hu, H.M. Meng, J.Q. Zhang, and C.N. Cao, Degradation mechanism of long service life Ti/IrO_2-TiO_2 oxide anodes in sulphuric acid, *Corros. Sci.*, 44(2002), No.8, p.1656.

[14] T.A.F. Lassali, L.O.S. Bulhoes, L.M.C. Abeid, and J.F.C. Boodts, Surface characterization of thermally prepared, Ti-supported, Ir-based electrocatalysts containing Ti and Sn, *J. Electrochem. Soc.*, 144(1997), No.10, p.3348.

[15] L.K. Xu and J.D. Scantlebury, A study on the deactivation of an IrO_2-Ta_2O_5 coated titanium anode, *Corros. Sci.*, 2003(45), No.12, p.2729.

[16] J. Ribeiro and A.R. de Andrade, Investigation of the electrical properties, charging process, and passivation of RuO_2-Ta_2O_5 oxide films, *J. Electroanal. Chem.*, 592(2006), No.2, p.153.

[17] B.V. Tilak, V.I. Birss, J. Wang, C.P. Chen, and S.K. Rangarajan, Deactivation of thermally formed Ru/Ti oxide electrodes: an AC impedance characterization study, *J. Electrochem. Soc.*, 148(2001), No.9, p.112.

[18] V.A. Alves, L.A. da Silva, J.F.C. Boodts, *et al.*, Electrochemical impedance spectroscopic study of dimensionally stable anode corrosion, *J. Appl. Electrochem.*, 28(1998), No.9, p.899.